1   **Dry and warm conditions in Australia exacerbated by aerosol reduction in China**

6   Jiyuan Gao[1], Yang Yang[1*], Hailong Wang[2], Pinya Wang[1], Hong Liao[1]

14   [1]Joint International Research Laboratory of Climate and Environment Change (ILCEC), Jiangsu

15   Key Laboratory of Atmospheric Environment Monitoring and Pollution Control, Jiangsu

16   Collaborative Innovation Center of Atmospheric Environment and Equipment Technology,

17   School of Environmental Science and Engineering, Nanjing University of Information Science

18   and Technology, Nanjing, Jiangsu, China

19   [2]Atmospheric, Climate, and Earth Sciences Division, Pacific Northwest National Laboratory,

20   Richland, Washington, USA

26   *Correspondence to yang.yang@nuist.edu.cn

Abstract

A substantial decline in anthropogenic aerosols in China has been observed since the initiation of clean air actions in 2013. ~~Concurrently, Australia experienced anomalously dry and warm conditions since the 2010s.~~ This study reveals a linkage between aerosol reductions in China and ~~the drying and warming trends in Australia during 2013–2019 based on fully-coupled climate model simulations and multi-source observations~~Australia's drier and warmer conditions. Aerosol decline in China triggered alterations in temperature and pressure gradients between the two hemispheres, leading to intensified outflow from Asia towards the South Indian Ocean, strengthening the Southern Indian Subtropical High and its related Southern Trade Winds. Consequently, this atmospheric pattern resulted in a moisture divergence over Australia. The reduction in surface moisture further resulted in more surface energy being converted into sensible heat instead of evaporating as latent heat, warming the near-surface air. ~~Aerosol reductions in China are found to contribute to the decreases in precipitation and relative humidity and the increase in surface air temperature in Australia during 2013–2019.~~ The intensified dry and warm climate conditions ~~during 2013–2019~~ further caused the increase in wildfire risks during fire seasons in Australia. Our study illuminates the impact of distant aerosols on precipitation and temperature variations in Australia, offering valuable insights for drought and wildfire risk mitigation in Australia.

1 Introduction

Australia encompasses various climate zones, ranging from the tropical climate in the north to arid conditions in the interior and temperate climates in the south (Head et al., 2014). The continent is predominantly dry, receiving an average annual rainfall of less than 600 mm and less than 300 mm over half of the land. Evident long-term trends can be observed in Australia's historical rainfall records. These trends reveal a notable shift towards drier conditions across southern Australia (Dey et al., 2019a; Nicholls, 2006; Rauniyar and Power, 2020; Wasko et al., 2021), and an increase in rainfall before 2010 (Dey et al., 2019a, b; Evans et al., 2014; Nicholls, 2006; Rotstayn et al., 2007; Wasko et al., 2021) followed by a slight decreasing trend of rainfall after 2010 (CSIRO and BOM, 2022) in the northern Australia.

Precipitation in Australia is influenced by a variety of atmospheric circulation systems, including East Coast Lows (ECLs), the Australian-Indonesian Monsoon, tropical cyclones (TCs), fronts, and different modes of large-scale climate variabilities, such as the El Niño-Southern Oscillation (ENSO), Indian Ocean Dipole (IOD), Interdecadal Pacific Oscillation (IPO), Subtropical ridge (STR), Southern Annular Mode (SAM), and Madden Julian Oscillation (MJO) (Dey et al., 2019a; Risbey et al., 2009). The linkages between Australia's rainfall characteristics and these drivers could change in response to the internal natural variabilities and external anthropogenic forcings. Rauniyar and Power (2020) reported that the drier conditions across the southern Australia could be attributed to a combination of both decadal-scale natural variability and changes in large-scale atmospheric circulation patterns, which was linked to the escalating emissions of greenhouse gases (GHGs), while Rotstayn et al. (2007) found that the increased levels of rainfall in northern Australia before 2010 was linked to the increases in aerosols in Asia.

Human activities have led to a rise of global surface air temperature by approximately 1.29 °C (0.99 to 1.65 °C) from 1750 to 2019, mainly due to an enhanced greenhouse effect from increasing GHG emissions (IPCC, 2021). In addition to GHGs, human activities also emit a variety of aerosols and their gaseous precursors into the atmosphere. Since industrialization, there has been a significant rise in the levels of aerosols and precursors (Hoesly et al., 2018). Atmospheric aerosols are the second-largest anthropogenic climate forcer, exerting an overall cooling effect that partially masks the warming induced by GHGs. (IPCC, 2013, 2021). However, as anthropogenic

76 aerosols declined during the past decades in many countries of the world related to the clean air
77 actions, the associated "unmask" effect is likely to exacerbate GHG-induced warming (Kloster et
78 al., 2010). For example, in the 1980s, clean air actions were implemented in North America and
79 Europe, leading to a decrease in the emissions of aerosols and their precursors (Hoesly et al., 2018).
80 Reductions in aerosol emissions in the U.S. have led to changes in aerosol direct radiative forcing
81 (DRF) by 0.8 W m^{-2} and indirect radiative forcing (IRF) by 1.0 W m^{-2} over the eastern U.S. during
82 1980–2010 (Leibensperger et al., 2012). Similarly, aerosol decreases over Europe between the
83 1980s and 1990s have caused a change in regional DRF by 1.26 W m^{-2} (Pozzoli et al., 2011). In
84 China, the emissions of aerosols and their precursors have been reduced since 2013 due to the
85 implementation of Air Pollution Prevention and Control Action Plan. Dang and Liao (2019)
86 reported a 1.18 W m^{-2} change in DRF between 2012 and 2017 due to decreased aerosol levels over
87 eastern China. Gao et al. (2022) estimated a warming of 0.20 °C in China, 0.15 °C in North
88 America, and 0.14 °C in Europe, attributed to the decreases in aerosols during 2013–2019.

89 Monsoonal rainfall serves as a vital resource for agriculture, industry, and ecosystems across
90 the monsoon-affected regions, affecting approximately two-thirds of the world's population (B.
91 Wang et al., 2021). Apart from GHGs-induced warming (Cook and Seager, 2013) and nature
92 variabilities (e.g., ENSO) (Oh and Ha, 2015), aerosol also modulates monsoon system mainly
93 through changing land-sea temperature and pressure gradient. The impact of aerosols on Asian
94 monsoon has been widely investigated. Based on climate model simulations, Liu et al. (2023)
95 found that aerosol reductions in East Asia during 2013–2017 resulted in an approximately 5%
96 increase in the strength of the East Asian summer monsoon (EASM). The EASM is also reported
97 to enhance due to future aerosol reductions from 2000 to 2100 (Wang et al., 2016). Dong et al.
98 (2019) explored the effects of increased aerosol in Asia from 1970s to 2000s on atmospheric
99 circulation and rainfall patterns and found anomalous moisture convergence and increased
100 precipitation over the Maritime continent. Non-Asian aerosols also have an effect on South Asian
101 monsoon rainfall through changes in the interhemispheric temperature gradient and meridional
102 shifts of the Intertropical Convergence Zone (Bollasina et al., 2011, 2014; Cowan and Cai, 2011;
103 Undorf et al., 2018). Australia, especially in northern Australia, is largely affected by the Australian
104 monsoon, which is characterized by winds that blow from the southeast during cold season and
105 from the northwest during the warm season (Gallego et al., 2017; Heidemann et al., 2023).
106 Australia has a relatively low level of anthropogenic aerosols, which suggests that the impact of

107   domestic anthropogenic aerosols on Australian monsoon should not be significant. However, the

108   impact of remote aerosols on Australian monsoon have been investigated in previous studies, and

109   they reported that the increases in Asian aerosols could enhance rainfall in Australia through

110   increasing monsoonal winds towards Australia (Rotstayn et al., 2007; Fahrenbach et al., 2023).

111   Wildfires, which are uncontrolled fires spreading rapidly across natural landscapes, are

112   significantly influenced by meteorological conditions (He et al., 2019; Jones et al., 2022). In

113   Australia, these fires, also known as bushfires, present a major environmental and social threat

114   (Johnston et al., 2021; Ward et al., 2020). According to Dowdy (2020), the most favorable seasons

115   for wildfires in most regions of Australia are austral spring and summer. Key meteorological

116   factors such as extended periods of drought, elevated temperatures, low humidity, and strong winds

117   are crucial in determining the occurrence and intensity of wildfires (Zacharakis and Tsihrintzis,

118   2023). Under the recent historical climate change, Australia has witnessed a rise in extreme fire

119   weather conditions and an extended fire season (CSIRO and BOM, 2022).

120   Since the implementation of clean air policies in 2013, there has been a noticeable decrease

121   in aerosol levels in China (Zhang et al., 2019; Zheng et al., 2018). Numerous studies have shown

122   the local and global climate effects of the aerosol reductions in China (Dang and Liao, 2019; Gao

123   et al., 2022, 2023; Liu et al., 2023; Zheng et al., 2020). The Australian monsoonal wind patterns,

124   reported to be influenced by Asian aerosol emissions in the past decades (Rotstayn et al., 2007;

125   Fahrenbach et al., 2023), may have also influenced by the radiative effects due to the aerosol

126   decline in China. The objective of this study is to ~~assess~~explore how aerosol emission reductions

127   in China affect the ~~worsened dry~~climate and ~~warm conditions and associated~~ wildfire risk in

128   Australia ~~during 2013–2019~~ and to investigate the ~~possible linkage between the changes in climate~~

129   ~~conditions in Australia and anthropogenic aerosols~~underlying mechanisms driving these impacts.

130   **2 Methods**

131   **2.1 Observational and Reanalysis Data**

132   Ground-based observational data of near-surface $PM_{2.5}$ concentrations in China 2013–2019

133   are acquired from the China National Environmental Monitoring Centre (CNEMC), which offers

134   daily records of near-surface air pollutant concentrations for nearly 1800 sites. Aerosol Optical

135 Depth (AOD) data are obtained from the Moderate Resolution Imaging Spectroradiometer

136 (MODIS) Deep Blue retrieval (Hsu et al., 2013). These observational data are used for evaluating

137 the performance of model simulated aerosols.

138 ERA5, the fifth generation of the European Centre for Medium-range Weather Forecasts

139 (ECMWF) atmospheric reanalysis, is a comprehensive dataset that provides a detailed and globally

140 consistent view of the earth's atmospheric conditions over the past several decades (Hersbach et

141 al., 2020). In this study, ERA5 data are employed to evaluate the climate condition in Australia

142 and analyze its linkage with aerosol reductions in China during the 2013–2019 by using the 2-

143 meter temperature, total precipitation, relative humidity, cloud cover, wind fields, vertical velocity,

144 surface latent and sensible heat flux, and surface and top of the atmosphere (TOA) solar and

145 longwave radiative flux under both clear and all sky conditions.

146 The Global Precipitation Measurement (GPM) mission is a joint initiative by National

147 Aeronautics and Space Administration (NASA) and the Japan Aerospace Exploration Agency

148 (JAXA) aimed at providing accurate and frequent measurements of global precipitation

149 (Skofronick-Jackson et al., 2017). GPM includes a core satellite equipped with advanced radar and

150 microwave sensors, enabling the observation of rain and snowfall in real-time. The data are crucial

151 for understanding weather patterns, climate dynamics, and hydrological processes. The Global

152 Precipitation Climatology Project (GPCP) is an international initiative under the World Climate

153 Research Programme (WCRP) that integrates satellite and gauge-based observations to provide

154 long-term, global precipitation estimates (Adler et al., 2018). GPCP offers monthly and daily

155 precipitation datasets with global coverage, combining data from rain gauges, satellite infrared

156 (IR), and microwave sensors to enhance accuracy. Precipitation rate data from GPM and GPCP

157 are also used in the study. GPM provides higher temporal and spatial resolution data compared to

158 Global Precipitation Climatology Project (GPCP), making it more suitable for studies focused on

159 short-term precipitation variability and regional climate dynamics.

160 **2.2 Model Description and Experimental Design**

161 In this research, we conduct simulations to explore the impact of aerosols on climate using

162 the Community Earth System Model version 1 (CESM1). CESM1 simulates the major aerosols

163 including sulfate, black carbon (BC), primary organic matter (POM), secondary organic aerosol

164 (SOA), dust and sea salt in a four-mode Modal Aerosol Module (MAM4), as described in Liu et

165 al. (2016). CESM1 simulations are carried out with 30 vertical layers and a horizontal resolution

166 of 2.5° longitude by 1.9° latitude. In addition to the default model physics, several supplementary

167 features are incorporated into the model in this study to improve the model's performance in

168 simulating aerosol wet scavenging and convective transport (Wang et al., 2013).

169   The global anthropogenic emissions of aerosols and their precursors are obtained from the

170 Community Emissions Data System (CEDS) v_2021_04_21. In contrast to the prior CEDS

171 v_2016_07_26, which exhibits significant regional emission biases (Z. Wang et al., 2021), the

172 newer CEDS version of anthropogenic emissions of aerosols and precursors considers the

173 substantial reductions in emissions in China, related to the recent clean air actions since 2013 (Fig.

174 S1). Specifically, anthropogenic sulfur dioxide (SO_2), BC, and organic carbon (OC) emissions

175 decreased by −12.48, −0.30, and −0.21 Tg yr^{-1}, respectively, over China between 2013 and 2019.

176 Biogenic emissions are from the Model of Emissions of Gases and Aerosols from Nature version

177 2.1 (MEGAN v2.1) (Guenther et al., 2012), while the emissions from open biomass burning are

178 derived from the CMIP6 (Coupled Model Intercomparison Project Phase 6) (Van Marle et al.,

179 2017).

180   A series of model experiments are conducted using CESM1 with a fully-coupled model

181 configuration, as detailed in Table S1. In the baseline scenario (referred to as BASE),

182 anthropogenic emissions of aerosols and precursors are fixed at year 2013 worldwide. In CHN,

183 anthropogenic emissions of aerosols and precursors over China are fixed at year 2019, while

184 emissions in all other regions are remained at year 2013. In NAEU, the simulation is performed

185 with anthropogenic emissions of aerosols and precursors over North America and Europe set at

186 year 2019, while emissions in other regions remained at year 2013. In OTH, anthropogenic

187 emissions of aerosols and precursors in other regions except for China are set at year 2019, while

188 emissions in China are kept at year 2013. In SASEA, anthropogenic emissions of aerosols and

189 precursors over South Asia and Southeast Asia are fixed at year 2019, while emissions in other

190 regions remained at year 2013. Biogenic and biomass burning emissions worldwide in all

191 experiments are fixed at year 2013. To reduce model biases related to internal variability, three

192 ensemble members are conducted by perturbing the initial atmospheric temperature conditions.

193 All simulations are run for 150 years, with the last 100 years for detailed analysis. To additionally

194 examine the fast climate responses to aerosol reductions in China, supplementary atmosphere-only

195 experiments (BASE_FAST and CN_FAST) were conducted using the CESM1 atmospheric

196 component (CAM5) with prescribed sea surface temperatures and sea ice concentrations. These

197 simulations were run for 30 years, and the outputs from the last 15 years were analyzed.

198 **2.3 Model Evaluation**

199 To validate whether CESM1 can reproduce the aerosol reductions in China during the 2010s,

200 changes in simulated near-surface $PM_{2.5}$ concentrations (sum of sulfate, BC, POM, SOA, dust×0.1,

201 and sea-salt×0.25 following Turnock et al. (2020)) in China during 2013–2019 are compared with

202 the observations. Figure S2 shows spatial distributions of observed and modeled annual mean near-

203 surface $PM_{2.5}$ concentration changes over China (2017–2019 minus 2013–2015), which exhibited

204 a statistically significant correlation coefficient of 0.52 between simulations and observations.

205 However, the model underestimates the $PM_{2.5}$ concentration changes by 76% in China. The

206 considerable underestimation has been reported in many previous studies, resulting from coarse

207 model resolution, uncertainties in emissions of aerosols and precursor gases, strong aerosol wet

208 removal, and the model's deficiency in simulating nitrate and ammonium aerosols (Fan et al., 2018,

209 2022; Gao et al., 2022, 2023; Zeng et al., 2021). The model has a good capability in replicating

210 the spatial distribution of AOD changes in China during 2013–2019 (Fig. S3), as evidenced by a

211 high correlation coefficient of 0.83, but the model also exhibits an underestimation in the AOD

212 reductions by 69%. However, the apparent underestimation of absolute changes may largely stem

213 from the inherently low background aerosol concentrations in CESM1. When considering the

214 relative changes rather than absolute values, the bias appears much less pronounced (Fig. S4 and

215 Fig. S5).

216 Climate variables, including precipitation rate, surface air temperature, relative humidity,

217 total cloud cover, surface solar radiation, 10m wind speed, and surface and TOA net total radiative

218 fluxes under both clear and all sky conditions over Australia simulated by CESM1 model are also

219 compared with those from ERA5 reanalysis (Fig. S6–S8). The model demonstrates a good

220 performance in simulating Australian climate, with normalized mean bias (NMB) values

221 consistently below or near 40% for surface air temperature, relative humidity, total cloud cover,

222 surface downward solar radiation, and 10m wind speed, and surface and TOA net total radiative

223   fluxes, but it tends to overestimate annual precipitation by about 90%, especially over coastal

224   regions likely related to the coarse model resolution. The model accurately reproduces spatial

225   patterns of all climate variables, closely aligning with observations, as indicated by correlation

226   coefficients ranging from 0.7 to 1.0.

227   **2.4 Wildfire Risk Indices**

228   In this study, several climatological indices are used to indicate wildfire risk during fire

229   seasons (austral spring and summer, from September to February of the next year) in Australia

230   (Ren et al., 2022; Irmak et al., 2003; Seager et al., 2015; Sharples et al., 2009).

231   (i) Reference Potential Evapotranspiration (ET_0):

232   ET_0 is a climatological index used to estimate the amount of water that could potentially

233   evaporate and be transpired from the Earth's surface under specific meteorological conditions. The

234   calculation of ET_0 takes into account factors such as temperature (T, unit: °C), and surface

235   downward solar radiation (R_s, unit: W m^{-2}) to estimate the maximum amount of water loss due to

236   evaporation and transpiration. ET_0 is important in wildfire studies because it helps to gauge the

237   environmental moisture conditions and the potential for drought, which can be a significant factor

238   in wildfire risks assessment. ET_0 is given by the following expression (Irmak et al., 2003):

239
$$ET_0 = -0.611 + 0.149R_s + 0.079\text{T}$$

240   (ii) Vapor Pressure Deficit (VPD):

241   Vapor Pressure Deficit (VPD) is a meteorological parameter that measures the difference

242   between the amount of moisture in the air and the maximum amount of moisture the air can hold

243   at a given temperature (T, unit: °C) and moisture (relative humidity, RH, unit: %). High VPD

244   values indicate that the air is dry. VPD is important in the context of wildfires because it reflects

245   the drying potential of the atmosphere. When VPD is high, it can lead to rapid moisture loss from

246   vegetation, making it more susceptible to ignition and increasing the risk of wildfires. VPD is

247   given by (Seager et al., 2015):

248
$$VPD = \frac{100 - RH}{100} \times 610.7 \times 10^{\frac{7.5T}{237.3+T}}$$

249   (iii) McArthur Forest Fire Danger Index (FFDI):

250   The McArthur Forest Fire Danger Index (FFDI) is a widely used index in Australia to assess

251   the potential for bushfires and forest fires. It takes into account various meteorological factors,

252   including T (unit: °C), RH (unit: %), wind speed (U, unit: m s^{-1}), and drought factor (DF, unitless).

253   We set DF as 10 here following Sharples et al. (2009), as it would not significantly affect the

254   methods of comparison used later in their study. While we acknowledge that this assumption is

255   idealized, we find it applicable in our case. To verify this, we calculated gridded DFs for Australia

256   (Figure S9), which show that the DFs are close to 10 and exhibit nearly homogeneous spatial

257   distributions. As such, setting DF = 10 for Australia is reasonable for our analysis. In addition,

258   FFDI calculated using DF = 10 and FFDI using gridded DFs are compared (Figure S10). The

259   patterns and regional averages of both datasets are very similar, further supporting the use of DF

260   = 10 in our study. The FFDI provides a numerical rating that indicates the level of fire danger,

261   with higher values corresponding to greater fire risks. This index is particularly valuable for

262   assessing the immediate risk of wildfires and is commonly used in fire management and prediction.

263   FFDI is defined as (Sharples et al., 2009):

264     $$FFDI = 2e^{-0.45+0.987lnDF+0.0338T-0.0345RH+0.0234U}$$

265   **3 Results**

266   **3.1 Intensified Dry and Warm Conditions in Australia by aerosol changes**

267   Figure 1 shows simulated responses in annual precipitation rate, surface air temperature and

268   relative humidity in Australia to changes in anthropogenic emissions of aerosols and precursors.

269   In response to aerosol reductions in China, Australia experiences significant decreases in

270   precipitation and relative humidity, while the temperature has an increase from 2013 to 2019. On

271   regional average, annual precipitation, surface air temperature and relative humidity change by –

272   0.10 mm day^{-1}, 0.06 °C, and –1.20%, respectively, in Australia caused by the aerosol reduction in

273   China during this time period, contributing to the dry and warm climate in Australia. Notably,

274   Northern Australia experiences the most significant reduction in convective precipitation, whereas

275   Southern Australia has the greatest decline in large-scale precipitation related to the aerosol

276   reduction in China, as simulated by the CESM1 model (Fig. S11). The direction of seasonal

277 responses in precipitation rate, surface air temperature and relative humidity are the same as the

278 annual averages, with the largest changes occurring in austral spring (Fig. 2). Regarding the strong

279 seasonal component observed in the responses, there are two main contributing factors: (1) the

280 background seasonality of the Southern Hemisphere trade winds, and (2) the seasonality of China's

281 emission changes themselves. However, determining which of these factors dominates requires

282 further detailed quantitative analysis.

283   The intensified dry and warm conditions in Australia can also be seen in the observations,

284 as indicated by ERA5 reanalysis data (Fig. 3). Since 2010, precipitation and relative humidity

285 have significantly decreased in Australia, especially in Northern and Eastern Australia, at a rate of

286 0.086 mm day^{-1} yr^{-1} and 1.07% yr^{-1}, respectively, while surface air temperature has increased at a

287 rate of 0.17 °C yr^{-1}. In addition, Time series of precipitation have also been extended to cover

288 2001–2019, clearly showing an increasing precipitation trend during 2001–2010, followed by a

289 decreasing trend during 2010–2019 (Fig. S12). It is in accordance with the increasing aerosols in

290 China before 2010 and aerosol reduction in recent years. (Fig. S12). To account for the potential

291 influence of internal variability, particularly ENSO, which is a major driver of Australia's

292 precipitation variability (Fig. S13), the time series are also given after removing the influence of

293 Niño 3.4 index. The adjusted results exhibit a similar transition, confirming the robustness of the

294 observed drying trend since the 2010s (Fig. S12). The GPM and GPCP data also exhibit a similar

295 decreasing trend in precipitation over Australia (Fig. S14). The reduction in anthropogenic SO_2

296 emissions in China shows strong correlations with the decrease in precipitation and the increase in

297 temperature in Australia during 2010–2019 (Fig. S15). However, when extending the time frame

298 to the period before emissions reductions in China (1940–2019), the increase in temperature

299 becomes less pronounced, with a slight rise in precipitation and relative humidity, likely attributed

300 to greenhouse gas warming, which can serve as indication that the decrease in precipitation and

301 increase in temperature in Australia from 2010 to 2019 are not primarily caused by GHGs (Fig.

302 S16). To place the recent drying trend in a longer-term context, all 10-year precipitation trends in

303 ERA5 data from 1940 onwards were calculated. The 10-year trends (unit: mm day^{-1} year^{-1}) were

304 found to be +0.016 (1940–1949), –0.012 (1950–1959), +0.001 (1960–1969), +0.031 (1970–1979),

305 –0.002 (1980–1989), +0.030 (1990–1999), –0.032 (2000–2009), and –0.086 (2010–2019). These

306 results indicate that the drying trend during 2010–2019 was unusually large compared to other

307 decades since 1940, suggesting that despite the influence of internal variability, a pronounced

308 reduction in precipitation over Australia has been observed in recent years. The rainfall decrease

309 is consistent with changes in clouds. Spatial distributions of simulated changes in vertically-

310 integrated cloud cover are shown in Figure S17, indicating a reduction in clouds of all levels,

311 including high, mid-level, and low clouds. In addition, the spatial distributions of these changes

312 closely resemble the patterns of responses in precipitation and relative humidity.

313 Aerosol emissions have changed across the world rather than in China aloneglobally during

314 2013–2019, not only in China but also in regions such as those in Australia, South Asia, Southeast

315 Asia, North America and, Europe, which affectand Australia, affecting climate in both locallocally

316 and remote regions.remotely. Figure 1 also shows the changes in climate variables in Australia

317 due to changes in other regions except China. Theresulting from aerosol emission changes in these

318 regions. Emission changes in other regions except China yield aan overall decrease in precipitation

319 by 0.06 mm day^{-1}, an increase in temperature by 0.06 °C, and a decrease in relative humidity by

320 0.67%. In particular, North America and Europe Among them, aerosol emission changes, to some

321 extent, contribute to in South Asia and Southeast Asia yield the largest responses, with a decrease

322 in precipitation (by 0.0408 mm day^{-1}),, an increase in temperature (by 0.0406 °C), and a decrease

323 in relative humidity (by 0.87%. Emission changes in North America and Europe contribute to a

324 decrease in precipitation by 0.04 mm day^{-1}, an increase in temperature by 0.04 °C, and a decrease

325 in relative humidity by 0.41%) attributed to other regions (except China),%, although thethese

326 responses are mostly insignificant (Fig. 1).

3.2 Mechanisms of Dry and Warm conditions in Australia Amplified by Aerosol Reductions in China

329 The rising levels of Asian aerosols could influence the meridional temperature and pressure

330 gradients across the Indian Ocean and therefore affect monsoonal winds and rainfall in Australia

331 since the middle of the 20th century, as reported in several previous studies (Fahrenbach et al.,

332 2023; Rotstayn et al., 2007). Since 2013, aerosol levels in China have substantially decreased due

333 to clean air actions initiated by the Chinese government (Zhang et al., 2019). At the same time,

334 precipitation in Australia exhibited a declining trend, which could be partly attributed to the

335 decrease in China's anthropogenic aerosol forcing as quantified through CESM1 simulations.

336   Asian monsoon region is closely connected with the meridional Hadley circulation and zonal

337   Walker circulation through monsoon outflow to the South India ocean subtropical high (SISH) and

338   North Pacific subtropical high (NPSH) (Beck et al., 2018). Figure 4a illustrates the climatological

339   mean wind fields at 850 hPa, indicating the persistent existence of SISH in the Indian Ocean and

340   NPSH in the North Pacific. With reductions in aerosols in China, the sea surface temperature (SST)

341   increases in the North Pacific but decreases in the Indian Ocean (Fig. 4b), which is concurrent with

342   the northward shift of the Intertropical Convergence Zone (ITCZ) (Basha et al., 2015). Over Asia,

343   this migration of ITCZ is accompanied by the northward movement of the upper-tropospheric

344   subtropical zonal westerly jet (Chiang et al., 2015; Schiemann et al., 2009), which moves to the

345   north of the Tibetan Plateau. It then enhances the circulation pattern of the Tibetan high, redirects

346   the outflow from the Asian monsoon to the southern Indian Ocean subtropical high (Fig. 5c),

347   strengthens the SISH, and leads to the enhancement of the Southern Trade Winds (Fig. 5d). On

348   the other hand, the increase in SST in the North Pacific induces ascending motion around the 130°–

349   150°E and the subsequent descending motion around the 90°–110°E (Fig. 5b), with anomalous

350   westerly winds near the surface, leading to a weakening of NPSH along with a decrease in the

351   Northern Trade Winds (Fig. 5d). Note that, the descending motion partly compensates the

352   ascending motion related to the meridional circulation between 10°–30°N (Fig. 5c). The

353   mechanism of China's aerosol reductions on the large-scale 3D circulation in the Asia-Pacific

354   region is shown in Figure 6. The enhancement of the Southern Trade Winds further causes

355   moisture advection away from Australia, accompanied by moisture divergence in Australia,

356   especially over the northern Australia (Fig. S18). This moisture divergence in Australia then

357   intensifies the dryness in Australia (Fig. 1).

358   Figures 7 illustrate the changes in relevant radiative fluxes in Australia resulting from

359   aerosol changes in China. Under the clear sky condition, both surface and top of the atmosphere

360   (TOA) radiative flux decrease (Fig. 7c&d). It is due to increased sea salt and dust aerosols (Fig.

361   S19b–d) due to the stronger Southern Trade Winds (Figs. S19a and 5d) and dryer conditions (Fig.

362   1). The decrease in cloud cover (Fig. S17) leads to an overall increase in both surface and TOA

363   radiative flux (Fig. 7e&f). The overall changes in radiative fluxes are offset by these two factors

364   (Fig. 7a&b) and insufficient to explain the significant increase in surface air temperature in

365   Australia (Fig. 1).

366   Decreases in precipitation lead to a decrease in surface specific humidity (Fig. S20a), which
367 declines more than that at 850 hPa (Fig. S20b). This results in excess energy being converted into
368 sensible heat rather than latent heat through evaporation (Chiang et al., 2018; Fischer et al., 2007;
369 Seneviratne et al., 2006; Su et al., 2014), which is indicated by a decrease in surface upward latent
370 heat flux and an increase in surface upward sensible heat flux in Australia due to aerosol changes
371 in China in Figure 8. The increased surface upward sensible heat flux heats the near-surface air
372 and contributes to the warm conditions in Australia.

3.3 Increases in Wildfire Risk in Australia

374   Wildfires represent a biosphere-atmosphere phenomenon, arising from the intricate interplay
375 of weather, climate, fuels, and human activities (Moritz et al., 2014). Notably, wildfires are ranked
376 among the most significant natural disasters in Australia, causing extensive damage (Shi et al.,
377 2021). Collins et al. (2022) reported that warmer and drier conditions increased the potential for
378 large and severe wildfire in Australia. Given that changes in aerosols in China have led to a warmer
379 and drier climate condition in Australia in recent years, the change in this climate state could also
380 impact on the occurrence of wildfires. Three wildfire risk indices (ET_0, VPD, and FFDI) are
381 selected to assess the risks of wildfires occurrence. Detailed information about the three wildfire
382 risk indices can be found in the Methods section.

383   All three indices exhibit increases (+0.37 mm mon^{-1} for ET_0, +0.56 hPa for VPD, and +0.25
384 for FFDI) during fire seasons (September to February) in Australia due to changes in aerosols in
385 China during 2013–2019 (Fig. 9), although they do not show the same spatial distribution possibly
386 due to different considerations regarding climate variables in the indices.

4 Conclusions and Discussions

388   This study reveals ~~a plausible connection between~~ that the substantial aerosol reduction in
389 China can lead to drier and ~~drying and warming trends~~ warmer conditions in Australia ~~that~~
390 ~~happened during the 2010s~~. Aerosol reductions in China induce changes in temperature and
391 pressure gradients, which lead to an increased outflow from Asia towards the South Indian Ocean,
392 strengthening the SISH and the associated Southern Trade Winds. Consequently, this atmospheric
393 pattern results in moisture divergence over Australia, causing a decrease in humidity and

394 precipitation. The reduction in surface moisture leads to more surface energy being converted into

395 sensible heat, rather than evaporating as latent heat, thereby heating the near-surface air. This

396 perspective sheds light on the influence of distant aerosols on climate in Australia.

397 The CESM1 simulations depict warmer and drier conditions in Australia related to China's

398 aerosol reductions than otherwise, a pattern also evident in observations represented by ERA5.

399 ~~However, it is important to note that China's aerosol reductions only contribute to a portion of the~~

400 ~~observed warm and dry conditions in Australia. Nonetheless~~It should be noted that the short-term

401 precipitation trends examined in this study may be influenced by internal climate variability,

402 especially given the relatively short period since 2013. Therefore, we extended the analysis back

403 to around 2010, when emission reductions in China had already begun. We also performed

404 additional analysis examining different time periods, including the 2013–2019 period (Fig. S21)

405 and a longer period (2010–2023; Fig. S22). Both patterns consistently show a decreasing trend in

406 Australia's precipitation, supporting the robustness of the recent drying trend in Australia.

407 However, we acknowledge that these observed short-term trends could still be affected by internal

408 climate variability, and the potential contribution from internal variability should not be ignored.

409 Although aerosol reductions may contribute to worsened climate conditions in Australia, air

410 quality and human health improvements owing to aerosol reductions cannot be ignored (Giani et

411 al., 2020; Zheng et al., 2017). In addition, the ~~drying~~drier and ~~warming trends~~warmer conditions

412 in Australia ~~attributed~~ linked to aerosol reductions should be considered resulting from the rise in

413 long-lived GHGs, while the aerosol reductions unmask the effect rooted in the GHGs (Wang et al.,

414 2023). In addition, other factors such as internal climate variability (Heidemann et al., 2023) appear

415 to have contributed more to the changes in Australia's climate conditions.

416 Rotstayn et al. (2007) and Fahrenbach et al. (2023) investigated the impact of increasing

417 anthropogenic aerosols over Asia during the late 20th century and early 21st century and indicated

418 that enhanced aerosol emissions strengthened the meridional temperature and pressure gradients,

419 intensifying the monsoonal circulation and leading to increased precipitation over Australia. In

420 contrast, our study focuses on the ~~recent~~ reductions in anthropogenic aerosols in China~~since 2013~~,

421 showing that the aerosol reductions reversed circulation changes induced by the previous aerosol

422 increases and ~~contributed~~led to drying rather than increased rainfall over Australia. Our study also

423   explores the subsequent impact of aerosol reductions in China on Australian temperature. We find

424   that reduced moisture availability over Australia led to a shift in surface energy partitioning, with

425   more energy being converted into sensible heat rather than latent heat, resulting in near-surface

426   warming. In summary, while previous studies have demonstrated the role of increasing Asian

427   aerosols in enhancing Australia's precipitation, our work complements these findings by showing

428   that decreasing aerosols, particularly from China, can drive the opposite effect, ~~contributing~~leading

429   to both ~~drying~~drier and ~~warming~~warmer conditions in Australia.

430   Liu et al. (2018) used multi-model simulations to investigate the fast and slow precipitation

431   responses to regional aerosol forcing from Asia and Europe under the PDRMIP framework. They

432   showed that Asian sulfate aerosols are strong drivers of global temperature and precipitation

433   changes, with fast precipitation responses scaling with atmospheric absorption and slow responses

434   scaling with surface temperature. However, their analysis focused on aerosol forcing from the

435   entire Asian region, rather than emission reductions from China alone, and the precipitation

436   responses over Australia were not significant in their results. Hwang et al. (2024) explored the

437   combined fast and slow climate responses to aerosol emission changes at the global scale. They

438   highlighted that fast adjustments of atmospheric circulation and joint feedback between low clouds,

439   wind, evaporation, and sea surface temperature, followed by slower oceanic responses, can sustain

440   La Niña-like cooling patterns in the equatorial Pacific for decades. However, neither study

441   specifically examined the climate impacts of China's recent emission reductions.

442   We acknowledge that fast and slow climate responses can have different mechanisms and

443   regional impacts, and there can be differences between the slow and fast responses. Both fast and

444   slow climate responses contribute to the simulated precipitation changes in Australia resulting

445   from China's emission reductions. Fast responses are primarily driven by rapid atmospheric

446   adjustments to aerosol-induced radiative forcing without requiring full ocean adjustment, while

447   slow responses involve gradual changes mediated by ocean circulation and sea surface temperature

448   adjustments over longer timescales. In our additional fast response experiments using the CAM5

449   atmospheric component, we found a decreasing pattern in Australia's precipitation (Fig. S23),

450   which is consistent with the long-term equilibrium simulation results. Although the equilibrium

451   simulations represent the fully adjusted climate system response and are not appropriate to be

452   directly compared to short-term observational changes, the fast response experiments suggest that

453 fast response accounts for 86% of the fully climate response in the changing precipitation in
454 Australia. It demonstrates that the immediate atmospheric response to Chinese aerosol reductions
455 alone can produce a drying effect similar to that found in long-period equilibrium experiments,
456 providing confidence in the robustness of the results.

457 One limitation of this study is the use of equilibrium experiments. Although the equilibrium
458 method is useful for isolating aerosol-induced climate responses, it does not fully capture the
459 transient climatic evolution. Attributing observed climate changes directly to modeled aerosol-
460 induced responses involves inherent uncertainties. Given the uncertainties, here we did not attempt
461 to quantitatively attribute the observed climate change to aerosols in this study, but showed the
462 mechanisms that how aerosol decline influence remote climate. Future work could also consider
463 transient simulations, which can better represent the role of aerosols in the climatic evolution of
464 the real world.

465 There are some other potential uncertainties in this study. Firstly, the low bias in simulated
466 aerosol concentrations in CESM1 and CESM1's larger sensitivity to aerosol forcing could
467 introduce some uncertainties. Secondly, our findings are derived from simulations conducted with
468 a single fully-coupled climate model, and it is vital for future research to employ multi-model
469 ensemble simulations to reduce the possibility of model-dependent specific results. While the
470 CMIP6 and PDRMIP (Precipitation Driver Response Model Intercomparison Project) can assist
471 in minimizing such model dependencies, they also present certain drawbacks. Anthropogenic
472 emissions input in CMIP6 inadequately accounts for aerosol reductions resulting from clean air
473 actions in China since 2013 (Z. Wang et al., 2021). Additionally, CMIP6 considers aerosol changes
474 globally, making it challenging to isolate effects specifically induced by changes in aerosols in
475 China. The experimental design of PDRMIP, which scales the concentrations of sulfate and BC in
476 Asia to ten times of their present-day levels, is generally idealistic and may not accurately and
477 proportionally represent aerosol changes observed in the real world. Finally, in addition to aerosols,
478 GHGs and nature variabilities also contribute to regional and global climate change. The extent to
479 which GHGs and nature variabilities could contribute to weather condition and climate changes in
480 Australia remains unknown, which warrants further investigation.

Nonetheless, our study examined ~~the role of~~how China's aerosol reductions ~~in~~could affect Australia's ~~recent drying and warming trends~~climate condition changes. Substantial emission reductions will continue in China following the carbon neutral pathway (Yang et al., 2023), while future changes in emissions in South Asia remain uncertain (Samset et al., 2019). Apart from natural climate variabilities that affect the Australian monsoon, further investigation of changes in monsoon precipitation in Australia should also consider the effects of remote aerosol changes simultaneously, which is crucial to effective drought and wildfire management and mitigation in Australia.

Acknowledgments

This study was supported by the National Natural Science Foundation of China (grant no. 42475032), the Jiangsu Science Fund for Carbon Neutrality (grant no. BK20220031), ~~and~~ Jiangsu Innovation and Entrepreneurship Team (grant no. JSSCTD202346~~). H.W. acknowledges the support of the U.S. Department of Energy (DOE), Office of Science, Office of Biological and Environmental~~), and Postgraduate Research ~~(BER), as part of the Earth and Environmental System Modeling program.~~Practice Innovation Program of Jiangsu Province (Grand KYCX25_1669). The Pacific Northwest National Laboratory (PNNL) is operated for DOE by the Battelle Memorial Institute under contract DE-AC05-76RLO1830.

Data and Code Availability

Ground-based observed PM$_{2.5}$ concentrations from CNEMC are available at https://quotsoft.net/air/ (last access: September 2024). AOD from MODIS Deep Blue retrieval are available at https://modis.gsfc.nasa.gov/ (last access: September 2024). ERA5 reanalysis data are available at https://cds.climate.copernicus.eu/ (last access: September 2024). GPM data are available at https://disc.gsfc.nasa.gov/datasets/GPM_3IMERGM_07/summary?keywords=%22IMERG%20final%22 (last access: September 2024). GPCP data are available at https://psl.noaa.gov/data/gridded/data.gpcp.html (last access: April 2025). The source code of CESM is available at https://github.com/ESCOMP/CESM (last access: September 2024). Our model results can be available at https://doi.org/10.5281/zenodo.13682943 (last access: September 2024).

Author Contributions

510

511 Y.Y. conceived the research and directed the analysis. J.G. conceived the research, conducted
512 the model simulations, and performed the analysis. All the authors including H.W., P.W., and H.
513 L. discussed the results and wrote the paper.

Competing Interests

514

515 At least one of the (co-)authors is a member of the editorial board of Atmospheric Chemistry
516 and Physics. The peer-review process was guided by an independent editor, and the authors also
517 have no other competing interests to declare.

References

518

519 Adler, R., Sapiano, M., Huffman, G., Wang, J.-J., Gu, G., Bolvin, D., Chiu, L., Schneider, U.,
520 Becker, A., Nelkin, E., Xie, P., Ferraro, R., and Shin, D.-B.: The Global Precipitation
521 Climatology Project (GPCP) Monthly Analysis (New Version 2.3) and a Review of 2017
522 Global Precipitation, Atmosphere, 9, 138, https://doi.org/10.3390/atmos9040138, 2018.

523 Basha, G., Kishore, P., Venkat Ratnam, M., Ouarda, T. B. M. J., Velicogna, I., and Sutterley, T.:
524 Vertical and latitudinal variation of the intertropical convergence zone derived using GPS
525 radio occultation measurements, Remote Sens. Environ., 163, 262–269,
526 https://doi.org/10.1016/j.rse.2015.03.024, 2015.

527 Beck, J. W., Zhou, W., Li, C., Wu, Z., White, L., Xian, F., Kong, X., and An, Z.: A 550,000-year
528 record of East Asian monsoon rainfall from 10Be in loess, Science, 360, 877–881,
529 https://doi.org/10.1126/science.aam5825, 2018.

530 Boer, M. M., Resco De Dios, V., and Bradstock, R. A.: Unprecedented burn area of Australian
531 mega forest fires, Nat. Clim. Change, 10, 171–172, https://doi.org/10.1038/s41558-020-
532 0716-1, 2020.

533 Bollasina, M. A., Ming, Y., and Ramaswamy, V.: Anthropogenic Aerosols and the Weakening of
534 the South Asian Summer Monsoon, Science, 334, 502–505,
535 https://doi.org/10.1126/science.1204994, 2011.

536 Bollasina, M. A., Ming, Y., Ramaswamy, V., Schwarzkopf, M. D., and Naik, V.: Contribution of
537 local and remote anthropogenic aerosols to the twentieth century weakening of the South
538 Asian Monsoon, Geophys. Res. Lett., 41, 680–687, https://doi.org/10.1002/2013GL058183,
539 2014.

Chiang, F., Mazdiyasni, O., and AghaKouchak, A.: Amplified warming of droughts in southern United States in observations and model simulations, Sci. Adv., 4, eaat2380, https://doi.org/10.1126/sciadv.aat2380, 2018.

Chiang, J. C. H., Fung, I. Y., Wu, C.-H., Cai, Y., Edman, J. P., Liu, Y., Day, J. A., Bhattacharya, T., Mondal, Y., and Labrousse, C. A.: Role of seasonal transitions and westerly jets in East Asian paleoclimate, Quat. Sci. Rev., 108, 111–129, https://doi.org/10.1016/j.quascirev.2014.11.009, 2015.

Collins, L., Clarke, H., Clarke, M. F., McColl Gausden, S. C., Nolan, R. H., Penman, T., and Bradstock, R.: Warmer and drier conditions have increased the potential for large and severe fire seasons across south-eastern Australia, Glob. Ecol. Biogeogr., 31, 1933–1948, https://doi.org/10.1111/geb.13514, 2022.

Cook, B. I. and Seager, R.: The response of the North American Monsoon to increased greenhouse gas forcing, J. Geophys. Res.: Atmos., 118, 1690–1699, https://doi.org/10.1002/jgrd.50111, 2013.

Cowan, T. and Cai, W.: The impact of Asian and non-Asian anthropogenic aerosols on 20th century Asian summer monsoon: ASIAN MONSOON AND AEROSOLS, Geophys. Res. Lett., 38, L11703, https://doi.org/10.1029/2011GL047268, 2011.

CSIRO and BOM: State of the Climate 2022, 2022

Dang, R. and Liao, H.: Radiative Forcing and Health Impact of Aerosols and Ozone in China as the Consequence of Clean Air Actions over 2012–2017, Geophys. Res. Lett., 46, 12511–12519, https://doi.org/10.1029/2019GL084605, 2019.

Dey, R., Lewis, S. C., Arblaster, J. M., and Abram, N. J.: A review of past and projected changes in Australia's rainfall, WIREs Clim. Change, 10, e577, https://doi.org/10.1002/wcc.577, 2019a.

Dey, R., Lewis, S. C., and Abram, N. J.: Investigating observed northwest Australian rainfall trends in Coupled Model Intercomparison Project phase 5 detection and attribution experiments, Int. J. Climatol., 39, 112–127, https://doi.org/10.1002/joc.5788, 2019b.

Dong, B., Wilcox, L. J., Highwood, E. J., and Sutton, R. T.: Impacts of recent decadal changes in Asian aerosols on the East Asian summer monsoon: roles of aerosol–radiation and aerosol–cloud interactions, Clim. Dyn., 53, 3235–3256, https://doi.org/10.1007/s00382-019-04698-0, 2019.

Dowdy, A. J.: Seamless climate change projections and seasonal predictions for bushfires in Australia, J. South. Hemisph. Earth Syst. Sci., 70, 120–138, https://doi.org/10.1071/ES20001, 2020.

Evans, S., Marchand, R., and Ackerman, T.: Variability of the Australian Monsoon and Precipitation Trends at Darwin, J. Climate, 27, 8487–8500, https://doi.org/10.1175/JCLI-D-13-00422.1, 2014.

577 Fahrenbach, N. L. S., Bollasina, M. A., Samset, B. H., Cowan, T., and Ekman, A. M. L.: Asian
578   anthropogenic aerosol forcing played a key role in the multi-decadal increase in Australian
579   summer monsoon rainfall, J. Climate, 1, https://doi.org/10.1175/JCLI-D-23-0313.1, 2023.

580 Fan, T., Liu, X., Ma, P.-L., Zhang, Q., Li, Z., Jiang, Y., Zhang, F., Zhao, C., Yang, X., Wu, F., and
581   Wang, Y.: Emission or atmospheric processes? An attempt to attribute the source of large
582   bias of aerosols in eastern China simulated by global climate models, Atmos. Chem. Phys.,
583   18, 1395–1417, https://doi.org/10.5194/acp-18-1395-2018, 2018.

584 Fan, T., Liu, X., Wu, C., Zhang, Q., Zhao, C., Yang, X., and Li, Y.: Comparison of the
585   Anthropogenic Emission Inventory for CMIP6 Models with a Country-Level Inventory over
586   China and the Simulations of the Aerosol Properties, Adv. Atmos. Sci., 39, 80–96,
587   https://doi.org/10.1007/s00376-021-1119-6, 2022.

588 Fischer, E. M., Seneviratne, S. I., Lüthi, D., and Schär, C.: Contribution of land-atmosphere
589   coupling to recent European summer heat waves, Geophys. Res. Lett., 34, 2006GL029068,
590   https://doi.org/10.1029/2006GL029068, 2007.

591 Gao, J., Yang, Y., Wang, H., Wang, P., Li, H., Li, M., Ren, L., Yue, X., and Liao, H.: Fast climate
592   responses to emission reductions in aerosol and ozone precursors in China during 2013–2017,
593   Atmos. Chem. Phys., 22, 7131–7142, https://doi.org/10.5194/acp-22-7131-2022, 2022.

594 Gao, J., Yang, Y., Wang, H., Wang, P., Li, B., Li, J., Wei, J., Gao, M., and Liao, H.: Climate
595   responses in China to domestic and foreign aerosol changes due to clean air actions during
596   2013–2019, npj Clim. Atmos. Sci., 6, 160, https://doi.org/10.1038/s41612-023-00488-y,
597   2023.

598 Giani, P., Castruccio, S., Anav, A., Howard, D., Hu, W., and Crippa, P.: Short-term and long-term
599   health impacts of air pollution reductions from COVID-19 lockdowns in China and Europe:
600   a modelling study, Lancet Planet. Health, 4, e474–e482, https://doi.org/10.1016/S2542-
601   5196(20)30224-2, 2020.

602 Guenther, A. B., Jiang, X., Heald, C. L., Sakulyanontvittaya, T., Duhl, T., Emmons, L. K., and
603   Wang, X.: The Model of Emissions of Gases and Aerosols from Nature version 2.1
604   (MEGAN2.1): an extended and updated framework for modeling biogenic emissions, Geosci.
605   Model Dev., 5, 1471–1492, https://doi.org/10.5194/gmd-5-1471-2012, 2012.

606 He, T., Lamont, B. B., and Pausas, J. G.: Fire as a key driver of Earth's biodiversity, Biol. Rev.,
607   94, 1983–2010, https://doi.org/10.1111/brv.12544, 2019.

608 Head, L., Adams, M., McGregor, H. V., and Toole, S.: Climate change and Australia, WIREs Clim.
609   Change, 5, 175–197, https://doi.org/10.1002/wcc.255, 2014.

610 Heidemann, H., Cowan, T., Henley, B. J., Ribbe, J., Freund, M., and Power, S.: Variability and
611   long-term change in Australian monsoon rainfall: A review, WIREs Clim. Change, 14, e823,
612   https://doi.org/10.1002/wcc.823, 2023.

613 Hersbach, H., Bell, B., Berrisford, P., Hirahara, S., Horányi, A., Muñoz-Sabater, J., Nicolas, J.,
614   Peubey, C., Radu, R., Schepers, D., Simmons, A., Soci, C., Abdalla, S., Abellan, X., Balsamo,
615   G., Bechtold, P., Biavati, G., Bidlot, J., Bonavita, M., De Chiara, G., Dahlgren, P., Dee, D.,
616   Diamantakis, M., Dragani, R., Flemming, J., Forbes, R., Fuentes, M., Geer, A., Haimberger,
617   L., Healy, S., Hogan, R. J., Hólm, E., Janisková, M., Keeley, S., Laloyaux, P., Lopez, P.,
618   Lupu, C., Radnoti, G., De Rosnay, P., Rozum, I., Vamborg, F., Villaume, S., and Thépaut, J.:
619   The ERA5 global reanalysis, Q. J. R. Meteorol. Soc., 146, 1999–2049,
620   https://doi.org/10.1002/qj.3803, 2020.

621 Hoesly, R. M., Smith, S. J., Feng, L., Klimont, Z., Janssens-Maenhout, G., Pitkanen, T., Seibert,
622   J. J., Vu, L., Andres, R. J., Bolt, R. M., Bond, T. C., Dawidowski, L., Kholod, N., Kurokawa,
623   J., Li, M., Liu, L., Lu, Z., Moura, M. C. P., O'Rourke, P. R., and Zhang, Q.: Historical (1750–
624   2014) anthropogenic emissions of reactive gases and aerosols from the Community Emissions
625   Data System (CEDS), Geosci. Model Dev., 11, 369–408, https://doi.org/10.5194/gmd-11-
626   369-2018, 2018.

627 Hsu, N. C., Jeong, M. -J., Bettenhausen, C., Sayer, A. M., Hansell, R., Seftor, C. S., Huang, J., and
628   Tsay, S. -C.: Enhanced Deep Blue aerosol retrieval algorithm: The second generation, J.
629   Geophys. Res.: Atmos., 118, 9296–9315, https://doi.org/10.1002/jgrd.50712, 2013.

630 Huneeus, N., Denier Van Der Gon, H., Castesana, P., Menares, C., Granier, C., Granier, L., Alonso,
631   M., De Fatima Andrade, M., Dawidowski, L., Gallardo, L., Gomez, D., Klimont, Z., Janssens-
632   Maenhout, G., Osses, M., Puliafito, S. E., Rojas, N., Ccoyllo, O. S.-, Tolvett, S., and Ynoue,
633   R. Y.: Evaluation of anthropogenic air pollutant emission inventories for South America at
634   national and city scale, Atmos. Environ., 235, 117606,
635   https://doi.org/10.1016/j.atmosenv.2020.117606, 2020.

636 Hwang, Y.-T., Xie, S.-P., Chen, P.-J., Tseng, H.-Y., and Deser, C.: Contribution of anthropogenic
637   aerosols to persistent La Niña-like conditions in the early 21st century, Proc. Natl. Acad. Sci.,
638   121, e2315124121, https://doi.org/10.1073/pnas.2315124121, 2024.

639 IPCC: Climate Change 2013: The Physical Science Basis, 2013.

640 IPCC: Climate Change 2021: The Physical Science Basis, 2021.

641 Irmak, S., Irmak, A., Allen, R. G., and Jones, J. W.: Solar and Net Radiation-Based Equations to
642   Estimate Reference Evapotranspiration in Humid Climates, J. Irrig. Drain. Eng., 129, 336–
643   347, https://doi.org/10.1061/(ASCE)0733-9437(2003)129:5(336), 2003.

644 Johnston, F. H., Borchers-Arriagada, N., Morgan, G. G., Jalaludin, B., Palmer, A. J., Williamson,
645   G. J., and Bowman, D. M. J. S.: Unprecedented health costs of smoke-related PM2.5 from
646   the 2019–20 Australian megafires, Nat. Sustain., 4, 42–47, https://doi.org/10.1038/s41893-
647   020-00610-5, 2021.

648 Jones, M. W., Abatzoglou, J. T., Veraverbeke, S., Andela, N., Lasslop, G., Forkel, M., Smith, A.
649   J. P., Burton, C., Betts, R. A., van der Werf, G. R., Sitch, S., Canadell, J. G., Santín, C.,
650   Kolden, C., Doerr, S. H., and Le Quéré, C.: Global and Regional Trends and Drivers of Fire

Under Climate Change, Rev. Geophys., 60, e2020RG000726, https://doi.org/10.1029/2020RG000726, 2022.

Kloster, S., Dentener, F., Feichter, J., Raes, F., Lohmann, U., Roeckner, E., and Fischer-Bruns, I.: A GCM study of future climate response to aerosol pollution reductions, Clim. Dyn., 34, 1177–1194, https://doi.org/10.1007/s00382-009-0573-0, 2010.

Lau, K.-M. and Kim, K.-M.: Observational relationships between aerosol and Asian monsoon rainfall, and circulation, Geophys. Res. Lett., 33, 2006GL027546, https://doi.org/10.1029/2006GL027546, 2006.

Leibensperger, E. M., Mickley, L. J., Jacob, D. J., Chen, W.-T., Seinfeld, J. H., Nenes, A., Adams, P. J., Streets, D. G., Kumar, N., and Rind, D.: Climatic effects of 1950–2050 changes in US anthropogenic aerosols – Part 1: Aerosol trends and radiative forcing, Atmos. Chem. Phys., 12, 3333–3348, https://doi.org/10.5194/acp-12-3333-2012, 2012.

Liu, C., Yang, Y., Wang, H., Ren, L., Wei, J., Wang, P., and Liao, H.: Influence of Spatial Dipole Pattern in Asian Aerosol Changes on East Asian Summer Monsoon, J. Climate, 36, 1575–1585, https://doi.org/10.1175/JCLI-D-22-0335.1, 2023.

Liu, L., Shawki, D., Voulgarakis, A., Kasoar, M., Samset, B. H., Myhre, G., Forster, P. M., Hodnebrog, Ø., Sillmann, J., Aalbergsjø, S. G., Boucher, O., Faluvegi, G., Iversen, T., Kirkevåg, A., Lamarque, J.-F., Olivié, D., Richardson, T., Shindell, D., and Takemura, T.: A PDRMIP Multimodel Study on the Impacts of Regional Aerosol Forcings on Global and Regional Precipitation, J. Climate, 31, 4429–4447, https://doi.org/10.1175/JCLI-D-17-0439.1, 2018.

Liu, X., Ma, P.-L., Wang, H., Tilmes, S., Singh, B., Easter, R. C., Ghan, S. J., and Rasch, P. J.: Description and evaluation of a new four-mode version of the Modal Aerosol Module (MAM4) within version 5.3 of the Community Atmosphere Model, Geosci. Model Dev., 9, 505–522, https://doi.org/10.5194/gmd-9-505-2016, 2016.

Ming, Y. and Ramaswamy, V.: Nonlinear Climate and Hydrological Responses to Aerosol Effects, J. Climate, 22, 1329–1339, https://doi.org/10.1175/2008JCLI2362.1, 2009.

Moritz, M. A., Batllori, E., Bradstock, R. A., Gill, A. M., Handmer, J., Hessburg, P. F., Leonard, J., McCaffrey, S., Odion, D. C., Schoennagel, T., and Syphard, A. D.: Learning to coexist with wildfire, Nature, 515, 58–66, https://doi.org/10.1038/nature13946, 2014.

Nicholls, N.: Detecting and attributing Australian climate change: a review, Aust. Meteorol. Mag., 2006.

Oh, H. and Ha, K.-J.: Thermodynamic characteristics and responses to ENSO of dominant intraseasonal modes in the East Asian summer monsoon, Clim. Dyn., 44, 1751–1766, https://doi.org/10.1007/s00382-014-2268-4, 2015.

Pozzoli, L., Janssens-Maenhout, G., Diehl, T., Bey, I., Schultz, M. G., Feichter, J., Vignati, E., and Dentener, F.: Re-analysis of tropospheric sulfate aerosol and ozone for the period 1980–2005

using the aerosol-chemistry-climate model ECHAM5-HAMMOZ, Atmos. Chem. Phys., 11, 9563–9594, https://doi.org/10.5194/acp-11-9563-2011, 2011.

Rauniyar, S. P. and Power, S. B.: The Impact of Anthropogenic Forcing and Natural Processes on Past, Present, and Future Rainfall over Victoria, Australia, J. Climate, 33, 8087–8106, https://doi.org/10.1175/JCLI-D-19-0759.1, 2020.

Ren, L., Yang, Y., Wang, H., Wang, P., Yue, X., and Liao, H.: Widespread Wildfires Over the Western United States in 2020 Linked to Emissions Reductions During COVID-19, Geophys. Res. Lett., 49, e2022GL099308, https://doi.org/10.1029/2022GL099308, 2022.

Risbey, J. S., Pook, M. J., McIntosh, P. C., Wheeler, M. C., and Hendon, H. H.: On the Remote Drivers of Rainfall Variability in Australia, Mon. Wea. Rev., 137, 3233–3253, https://doi.org/10.1175/2009MWR2861.1, 2009.

Rotstayn, L. D., Cai, W., Dix, M. R., Farquhar, G. D., Feng, Y., Ginoux, P., Herzog, M., Ito, A., Penner, J. E., Roderick, M. L., and Wang, M.: Have Australian rainfall and cloudiness increased due to the remote effects of Asian anthropogenic aerosols?, J. Geophys. Res.: Atmos., 112, 2006JD007712, https://doi.org/10.1029/2006JD007712, 2007.

Samset, B. H., Lund, M. T., Bollasina, M., Myhre, G., and Wilcox, L.: Emerging Asian aerosol patterns, Nat. Geosci., 12, 582–584, https://doi.org/10.1038/s41561-019-0424-5, 2019.

Schiemann, R., Lüthi, D., and Schär, C.: Seasonality and Interannual Variability of the Westerly Jet in the Tibetan Plateau Region, J. Climate, 22, 2940–2957, https://doi.org/10.1175/2008JCLI2625.1, 2009.

Seager, R., Hooks, A., Williams, A. P., Cook, B., Nakamura, J., and Henderson, N.: Climatology, Variability, and Trends in the U.S. Vapor Pressure Deficit, an Important Fire-Related Meteorological Quantity, J. Appl. Meteorol. Clim., 54, 1121–1141, https://doi.org/10.1175/JAMC-D-14-0321.1, 2015.

Seneviratne, S. I., Lüthi, D., Litschi, M., and Schär, C.: Land–atmosphere coupling and climate change in Europe, Nature, 443, 205–209, https://doi.org/10.1038/nature05095, 2006.

Sharples, J. J., McRae, R. H. D., Weber, R. O., and Gill, A. M.: A simple index for assessing fire danger rating, Environ. Modell. Softw., 24, 764–774, https://doi.org/10.1016/j.envsoft.2008.11.004, 2009.

Shi, G., Yan, H., Zhang, W., Dodson, J., Heijnis, H., and Burrows, M.: Rapid warming has resulted in more wildfires in northeastern Australia, Sci. Total Environ., 771, 144888, https://doi.org/10.1016/j.scitotenv.2020.144888, 2021.

Skofronick-Jackson, G., Petersen, W. A., Berg, W., Kidd, C., Stocker, E. F., Kirschbaum, D. B., Kakar, R., Braun, S. A., Huffman, G. J., Iguchi, T., Kirstetter, P. E., Kummerow, C., Meneghini, R., Oki, R., Olson, W. S., Takayabu, Y. N., Furukawa, K., and Wilheit, T.: The Global Precipitation Measurement (GPM) Mission for Science and Society, Bull. Am. Meteorol. Soc., 98, 1679–1695, https://doi.org/10.1175/BAMS-D-15-00306.1, 2017.

Streets, D. G., Yan, F., Chin, M., Diehl, T., Mahowald, N., Schultz, M., Wild, M., Wu, Y., and Yu, C.: Anthropogenic and natural contributions to regional trends in aerosol optical depth, 1980–2006, J. Geophys. Res.: Atmos., 114, 2008JD011624, https://doi.org/10.1029/2008JD011624, 2009.

Su, H., Yang, Z., Dickinson, R. E., and Wei, J.: Spring soil moisture-precipitation feedback in the Southern Great Plains: How is it related to large-scale atmospheric conditions?, Geophys. Res. Lett., 41, 1283–1289, https://doi.org/10.1002/2013GL058931, 2014.

Turnock, S. T., Allen, R. J., Andrews, M., Bauer, S. E., Deushi, M., Emmons, L., Good, P., Horowitz, L., John, J. G., Michou, M., Nabat, P., Naik, V., Neubauer, D., O'Connor, F. M., Olivié, D., Oshima, N., Schulz, M., Sellar, A., Shim, S., Takemura, T., Tilmes, S., Tsigaridis, K., Wu, T., and Zhang, J.: Historical and future changes in air pollutants from CMIP6 models, Atmos. Chem. Phys., 20, 14547–14579, https://doi.org/10.5194/acp-20-14547-2020, 2020.

Undorf, S., Polson, D., Bollasina, M. A., Ming, Y., Schurer, A., and Hegerl, G. C.: Detectable Impact of Local and Remote Anthropogenic Aerosols on the 20th Century Changes of West African and South Asian Monsoon Precipitation, J. Geophys. Res.: Atmos., 123, 4871–4889, https://doi.org/10.1029/2017JD027711, 2018.

Van Marle, M. J. E., Kloster, S., Magi, B. I., Marlon, J. R., Daniau, A.-L., Field, R. D., Arneth, A., Forrest, M., Hantson, S., Kehrwald, N. M., Knorr, W., Lasslop, G., Li, F., Mangeon, S., Yue, C., Kaiser, J. W., and Van Der Werf, G. R.: Historic global biomass burning emissions for CMIP6 (BB4CMIP) based on merging satellite observations with proxies and fire models (1750–2015), Geosci. Model Dev., 10, 3329–3357, https://doi.org/10.5194/gmd-10-3329-2017, 2017.

Wang, B., Biasutti, M., Byrne, M. P., Castro, C., Chang, C.-P., Cook, K., Fu, R., Grimm, A. M., Ha, K.-J., Hendon, H., Kitoh, A., Krishnan, R., Lee, J.-Y., Li, J., Liu, J., Moise, A., Pascale, S., Roxy, M. K., Seth, A., Sui, C.-H., Turner, A., Yang, S., Yun, K.-S., Zhang, L., and Zhou, T.: Monsoons Climate Change Assessment, Bull. Am. Meteorol. Soc., 102, E1–E19, https://doi.org/10.1175/BAMS-D-19-0335.1, 2021.

Wang, H., Easter, R. C., Rasch, P. J., Wang, M., Liu, X., Ghan, S. J., Qian, Y., Yoon, J.-H., Ma, P.-L., and Vinoj, V.: Sensitivity of remote aerosol distributions to representation of cloud–aerosol interactions in a global climate model, Geosci. Model Dev., 6, 765–782, https://doi.org/10.5194/gmd-6-765-2013, 2013.

Wang, P., Yang, Y., Xue, D., Ren, L., Tang, J., Leung, L. R., and Liao, H.: Aerosols overtake greenhouse gases causing a warmer climate and more weather extremes toward carbon neutrality, Nat. Commun., 14, 7257, https://doi.org/10.1038/s41467-023-42891-2, 2023.

Wang, Z., Zhang, H., and Zhang, X.: Projected response of East Asian summer monsoon system to future reductions in emissions of anthropogenic aerosols and their precursors, Clim. Dyn., 47, 1455–1468, https://doi.org/10.1007/s00382-015-2912-7, 2016.

Wang, Z., Lin, L., Xu, Y., Che, H., Zhang, X., Zhang, H., Dong, W., Wang, C., Gui, K., and Xie, B.: Incorrect Asian aerosols affecting the attribution and projection of regional climate change

764   in CMIP6 models, npj Clim. Atmos. Sci., 4, 2, https://doi.org/10.1038/s41612-020-00159-2,
765   2021.

766 Ward, M., Tulloch, A. I. T., Radford, J. Q., Williams, B. A., Reside, A. E., Macdonald, S. L.,
767   Mayfield, H. J., Maron, M., Possingham, H. P., Vine, S. J., O'Connor, J. L., Massingham, E.
768   J., Greenville, A. C., Woinarski, J. C. Z., Garnett, S. T., Lintermans, M., Scheele, B. C.,
769   Carwardine, J., Nimmo, D. G., Lindenmayer, D. B., Kooyman, R. M., Simmonds, J. S., Sonter,
770   L. J., and Watson, J. E. M.: Impact of 2019–2020 mega-fires on Australian fauna habitat, Nat.
771   Ecol. Evol., 4, 1321–1326, https://doi.org/10.1038/s41559-020-1251-1, 2020.

772 Wasko, C., Shao, Y., Vogel, E., Wilson, L., Wang, Q. J., Frost, A., and Donnelly, C.:
773   Understanding trends in hydrologic extremes across Australia, J. Hydrol., 593, 125877,
774   https://doi.org/10.1016/j.jhydrol.2020.125877, 2021.

775 Yang, Y., Zeng, L., Wang, H., Wang, P., and Liao, H.: Climate effects of future aerosol reductions
776   for achieving carbon neutrality in China, Sci. Bull., 68, 902–905,
777   https://doi.org/10.1016/j.scib.2023.03.048, 2023.

778 Zacharakis, I. and Tsihrintzis, V. A.: Integrated wildfire danger models and factors: A review, Sci.
779   Total Environ., 899, 165704, https://doi.org/10.1016/j.scitotenv.2023.165704, 2023.

780 Zeng, L., Yang, Y., Wang, H., Wang, J., Li, J., Ren, L., Li, H., Zhou, Y., Wang, P., and Liao, H.:
781   Intensified modulation of winter aerosol pollution in China by El Niño with short duration,
782   Atmos. Chem. Phys., 21, 10745–10761, https://doi.org/10.5194/acp-21-10745-2021, 2021.

783 Zhang, Q., Zheng, Y., Tong, D., Shao, M., Wang, S., Zhang, Y., Xu, X., Wang, J., He, H., Liu,
784   W., Ding, Y., Lei, Y., Li, J., Wang, Z., Zhang, X., Wang, Y., Cheng, J., Liu, Y., Shi, Q., Yan,
785   L., Geng, G., Hong, C., Li, M., Liu, F., Zheng, B., Cao, J., Ding, A., Gao, J., Fu, Q., Huo, J.,
786   Liu, B., Liu, Z., Yang, F., He, K., and Hao, J.: Drivers of improved PM2.5 air quality in China
787   from 2013 to 2017, Proc. Natl. Acad. Sci., 116, 24463–24469,
788   https://doi.org/10.1073/pnas.1907956116, 2019.

789 Zheng, B., Tong, D., Li, M., Liu, F., Hong, C., Geng, G., Li, H., Li, X., Peng, L., Qi, J., Yan, L.,
790   Zhang, Y., Zhao, H., Zheng, Y., He, K., and Zhang, Q.: Trends in China's anthropogenic
791   emissions since 2010 as the consequence of clean air actions, Atmos. Chem. Phys., 18,
792   14095–14111, https://doi.org/10.5194/acp-18-14095-2018, 2018.

793 Zheng, Y., Xue, T., Zhang, Q., Geng, G., Tong, D., Li, X., and He, K.: Air quality improvements
794   and health benefits from China's clean air action since 2013, Environ. Res. Lett., 12, 114020,
795   https://doi.org/10.1088/1748-9326/aa8a32, 2017.

796 Zheng, Y., Zhang, Q., Tong, D., Davis, S. J., and Caldeira, K.: Climate effects of China's efforts
797   to improve its air quality, Environ. Res. Lett., 15, 104052, https://doi.org/10.1088/1748-
798   9326/ab9e21, 2020.
799

800

801
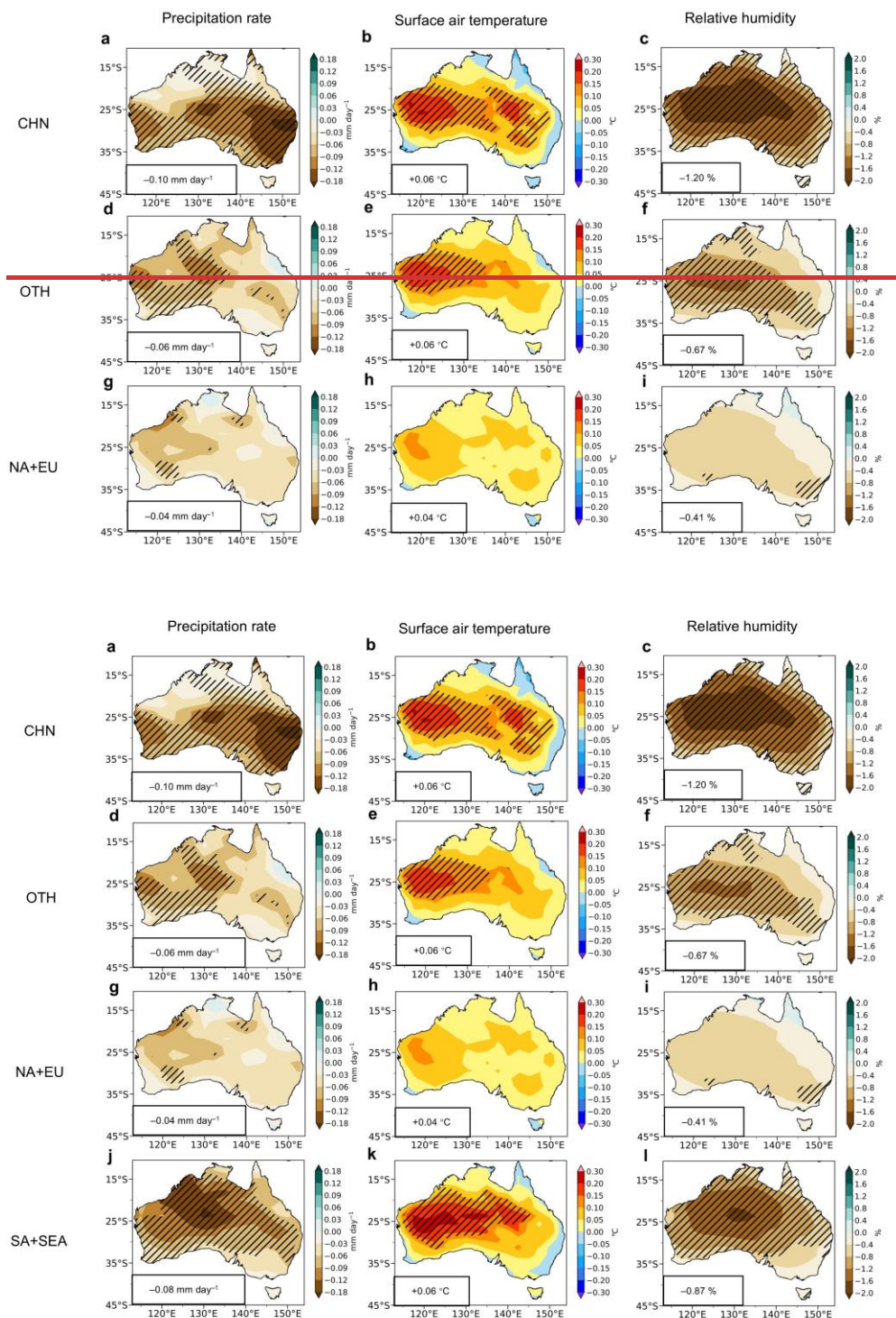
Figure 1. Simulated changes in precipitation rate, surface air temperature and relative humidity in Australia due to aerosol changes between 2013 and 2019. Spatial distributions of simulated differences in annual mean precipitation rate (Pr, **a**, **d**, and **g**, unit: mm day^{-1}), surface

air temperature (TS, **b**, **e**, and **h**, unit: °C) and relative humidity (RH, **c**, **f**, and **i**, unit: %) in

Australia between BASE and CHN (CHN minus BASE, **a**–**c**), between BASE and OTH (OTH

minus BASE, **d**–**f**), ~~and~~ between BASE and NAEU (NAEU minus BASE, **g**–i), and between

BASE and SASEA (SASEA minus BASE, **j**–**l**). The shaded areas indicate results are statistically

significant at the 90% confidence level. Regional averages over Australia are noted at the

bottom-left corner of each panel.
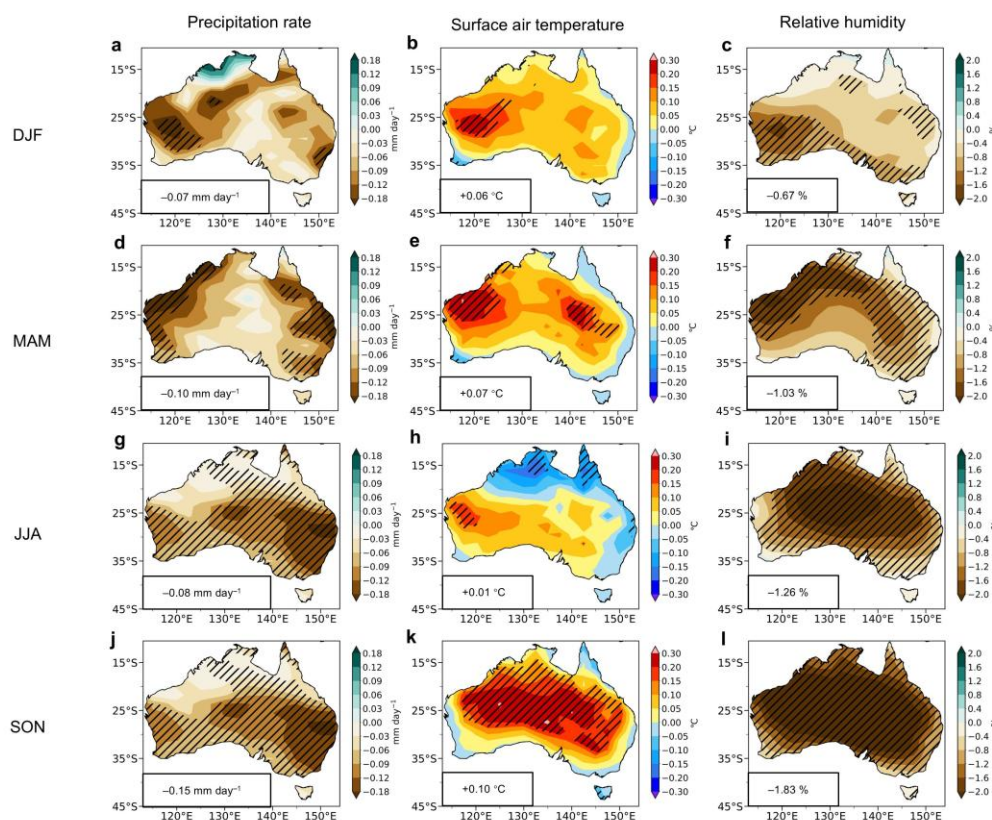
Figure 2. Simulated changes in precipitation rate, surface air temperature and relative

humidity in Australia due to aerosol changes in China between 2013 and 2019. Spatial

distributions of simulated differences in DJF (December, January and February, **a**–**c**), MAM

(March, April and May, **d**–**f**), JJA (June, July and August, **g**–**i**) and SON (September, October

and November, **j**–**l**) mean precipitation rate (Pr, **a**, **d**, **g**, and **j**, unit: mm day^{-1}), surface air

temperature (TS, **b**, **e**, **h**, and **k**, unit: °C) and relative humidity (RH, **c**, **f**, **i**, and **l**, unit: %) in

Australia between BASE and CHN (CHN minus BASE).The shaded areas indicate results are

statistically significant at the 90% confidence level. Regional averages over Australia are noted

at the bottom-left corner of each panel.

821

822
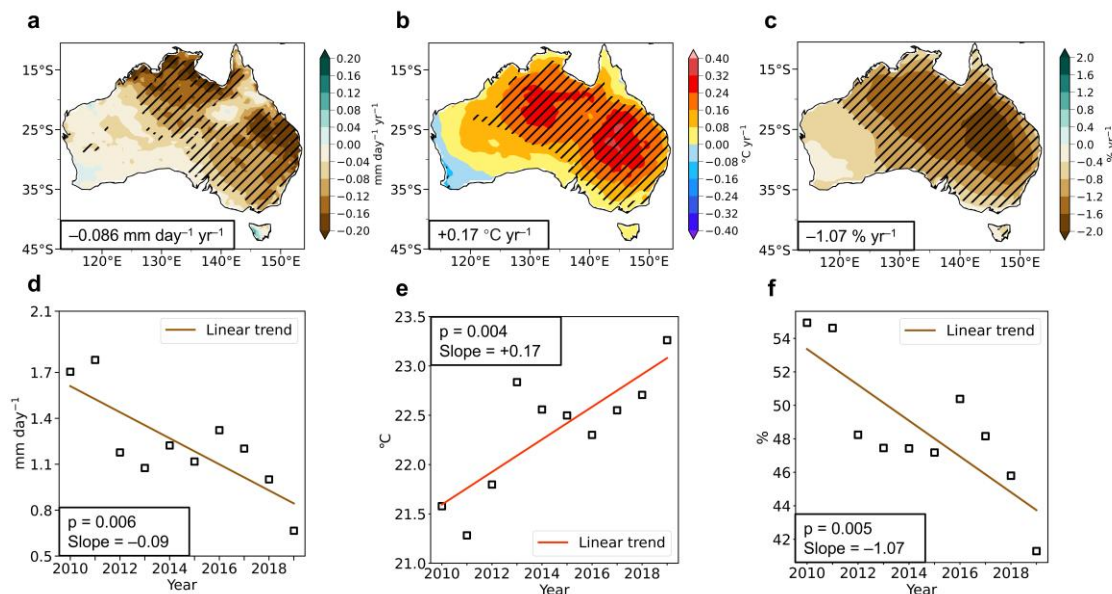
823 **Figure 3. Linear trends of observed precipitation rate, surface air temperature and relative**

824 **humidity in Australia based on ERA5.** Spatial distributions of linear trends (**a**, **b**, and **c**) and

825 time series (**d**, **e**, and **f**) of annual mean precipitation rate (Pr, **a** and **d**, unit: mm day^{-1}), surface air

826 temperature (TS, **b** and **e**, unit: °C) and relative humidity (RH, **c** and **f**, unit: %) in Australia during

827 2010–2019 from ERA5 reanalysis. The shaded areas indicate trends are statistically significant at

828 the 90% confidence level. Regional averages over Australia are noted at the bottom-left corner of

829 panels a, b, and c. The p values and slopes of linear trends are noted in panels d, e, and f.

830

831
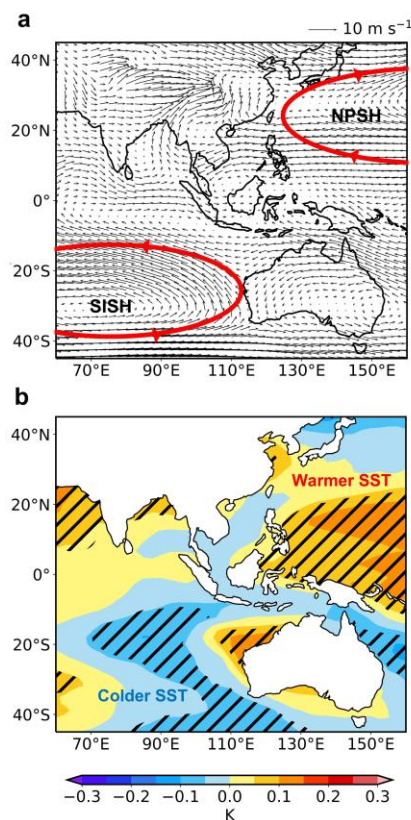
Figure 4. Climatological mean wind fields at 850 hPa and Simulated sea surface temperature changes due to aerosol changes in China between 2013 and 2019. a, Climatological mean wind fields (unit: m s^{-1}, vectors) at 850 hPa from the BASE experiment. NPSH and SISH shown in red circles represents North Pacific Subtropical High and Southern Indian ocean Subtropical High, respectively. **b**, Spatial distributions of simulated differences in annual mean sea surface temperature (SST, unit: mm day^{-1}) in Australia between BASE and CHN (CHN minus BASE). The shaded areas indicate results are statistically significant at the 90% confidence level.

839

840
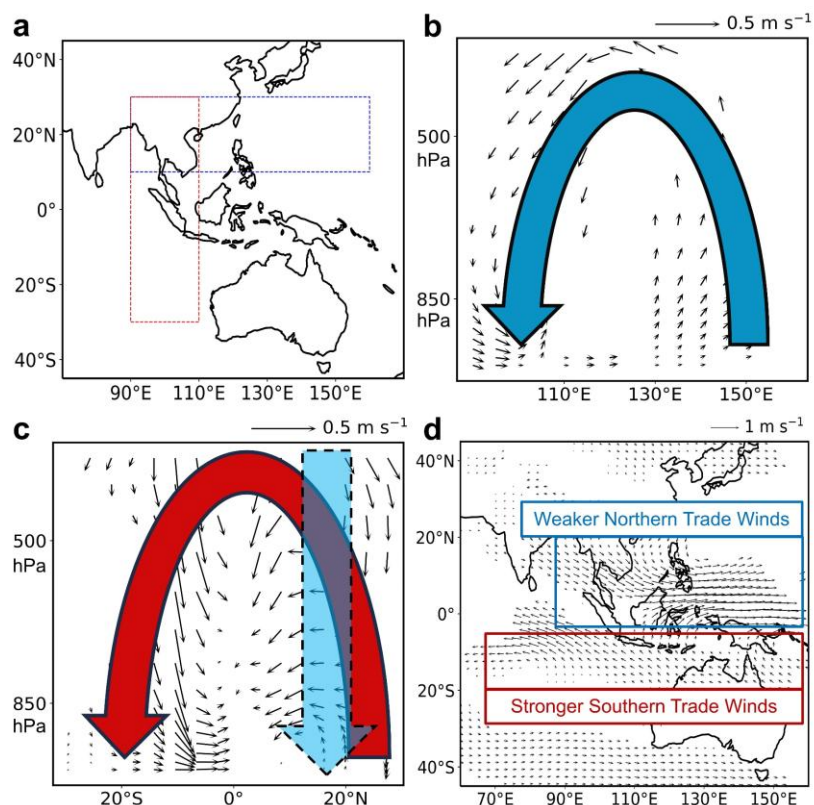
Figure 5. Simulated changes in vertical circulations and 850 hPa wind fields in Asia-Pacific regions due to aerosol changes in China between 2013 and 2019. Panel **b** and **c** shows pressure–longitude and pressure–latitude cross-section of responses in annual mean atmospheric circulations (unit: m s^{-1}, vectors), respectively, over the areas marked with the blue and red box in panel **a**. Panel **d** shows annual mean changes in wind fields (unit: m s^{-1}, vectors) at 850 hPa in Asia-Pacific regions. Only atmospheric circulations and winds statistically significant at the 90% confidence level are shown.

848

849
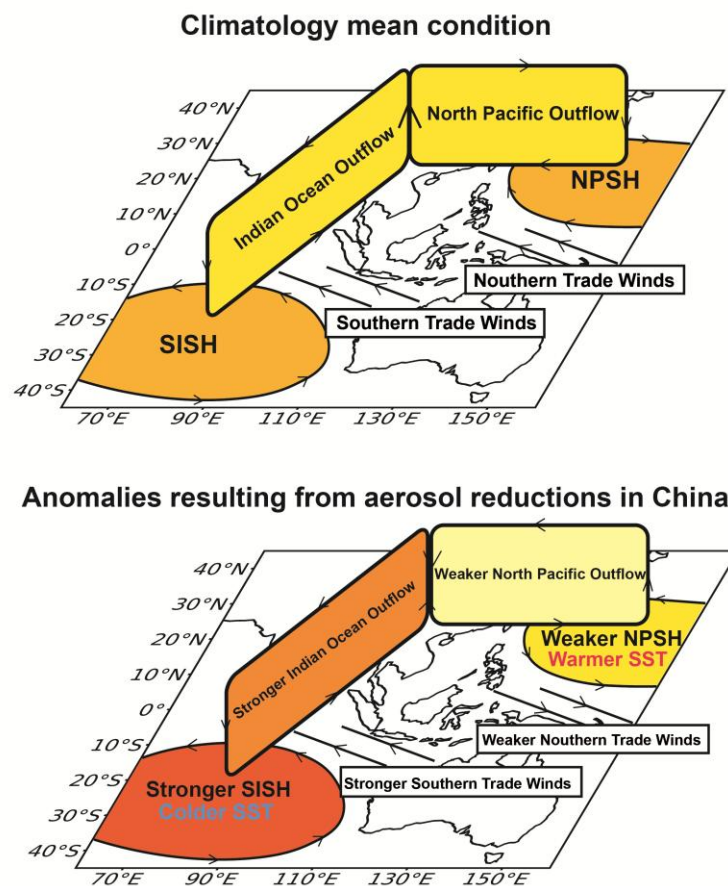
Figure 6. Schematic of the response in large-scale 3D circulations in the Asian-Pacific region to aerosol reductions in China. The top panel shows climatology mean condition, and the bottom panel shows anomalies resulting from aerosol reductions in China.

853
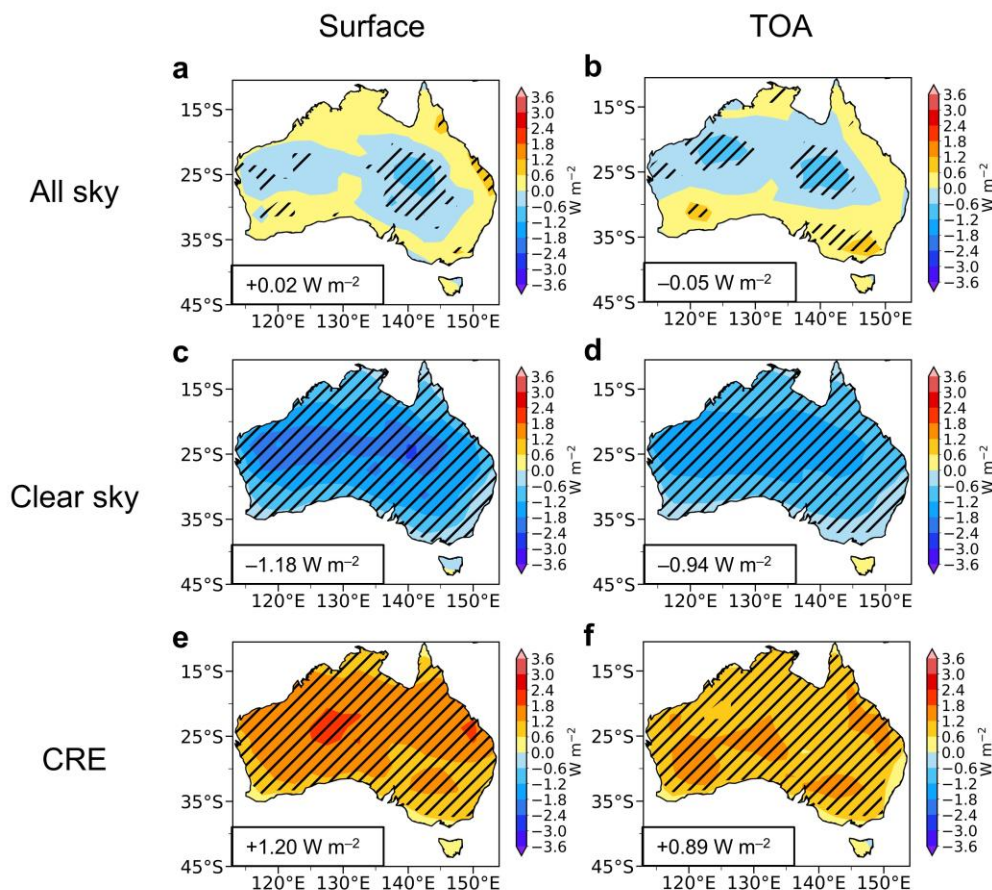
Figure 7. Simulated changes in surface and Top of the Atmosphere (TOA) net total radiative flux under all sky conditions, under clear sky conditions, and from cloud radiative effects in Australia due to aerosol changes in China between 2013 and 2019. Spatial distributions of simulated differences in annual mean surface (**a**, **c**, and **e**) and Top of the Atmosphere (TOA, **b**, **d**, and **f**) net total radiative flux (unit: W m^{-2}) under all sky conditions (**a** and **b**), under clear sky conditions (**c** and **d**), and from cloud radiative effects (CRE, **e** and **f**) in Australia between BASE and CHN (CHN minus BASE). Cloud radiative effects refer to differences under all sky and clear sky conditions (All sky minus Clear sky). The shaded areas indicate results are statistically significant at the 90% confidence level. Regional averages of the responses over Australia are noted at the bottom-left corner of each panel.

864
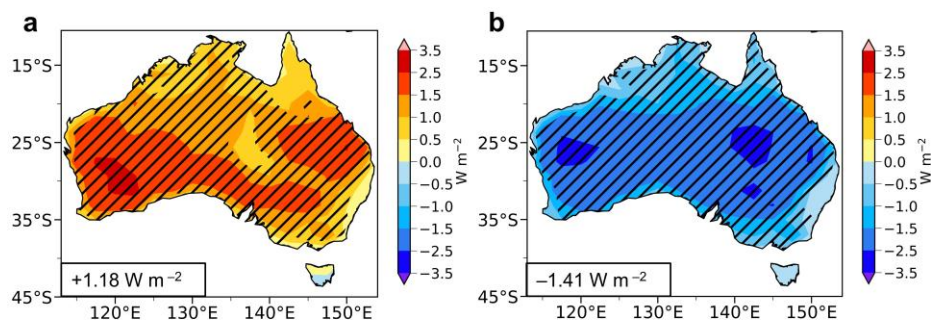
Figure 8. Simulated changes in surface upward sensible and latent heat flux in Australia due to aerosol changes in China between 2013 and 2019. Spatial distributions of simulated differences in annual mean surface upward sensible (**a**) and latent (**b**) heat flux (unit: W m^{-2}) in Australia between BASE and CHN (CHN minus BASE). The shaded areas indicate results are statistically significant at the 90% confidence level. Regional averages over Australia are noted at the bottom-left corner of each panel.

873
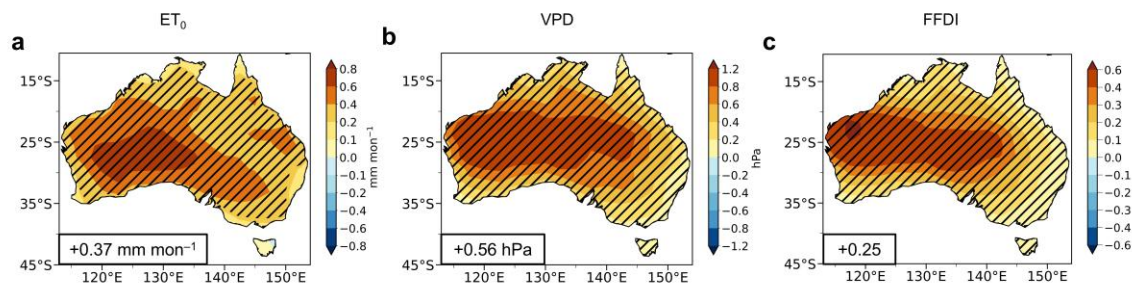
Figure 9. Simulated changes in reference potential evapotranspiration, vapor pressure deficit, and McArthur forest fire danger index during fire seasons in Australia due to aerosol changes in China between 2013 and 2019. Spatial distributions of simulated changes in reference potential evapotranspiration (ET$_0$, **a**, unit: mm mon^{-1}), vapor pressure deficit (VPD, **b**, unit: hPa), and McArthur forest fire danger index (FFDI, **c**, unitless) during fire seasons (austral spring and summer, from September to the February of the next year) in Australia between BASE and CHN (CHN minus BASE). The shaded areas indicate results are statistically significant at the 90% confidence level. Regional averages over Australia are noted at the bottom-left corner of each panel.